The Astrophysical Journal, 603:221–230, 2004 March 1

TOWARD GRAVITATIONAL WAVE SIGNALS FROM REALISTIC CORE-COLLAPSE SUPERNOVA MODELS

Ewald Müller, Markus Rampp, Robert Buras, and H.-Thomas Janka
Max-Planck-Institut für Astrophysik, Karl-Schwarzschild-Strasse 1, D-85740 Garching, Germany

and

David H. Shoemaker
Laser Interferometer Gravitational-Wave Observatory Laboratory, 175 St. Albany Street, Massachusetts Institute of Technology, Cambridge, MA 02139
Received 2003 October 2; accepted 2003 November 13

ABSTRACT

We have computed the gravitational wave signal from supernova core collapse by using the most realistic input physics available at present. We start from state-of-the-art progenitor models of rotating and nonrotating massive stars and simulate the dynamics of their core collapse by integrating the equations of axisymmetric hydrodynamics, together with the Boltzmann equation for the neutrino transport, including an elaborate description of neutrino interactions, and a realistic equation of state. Using the Einstein quadrupole formula we compute the quadrupole wave amplitudes, the Fourier wave spectra, the amount of energy radiated in the form of gravitational waves, and the signal-to-noise ratios for the Laser Interferometer Gravitational-Wave Observatory (LIGO) I and the tuned Advanced LIGO (LIGO II) interferometers resulting from both nonradial mass motion and anisotropic neutrino emission. The simulations demonstrate that the dominant contribution to the gravitational wave signal is produced by neutrino-driven convection behind the supernova shock. For stellar cores rotating at the extreme of current stellar evolution predictions, the core bounce signal is detectable ($S/N \gtrsim 7$) with LIGO II for a supernova up to a distance of $\sim$5 kpc, whereas the signal from postshock convection is observable ($S/N \gtrsim 7$) with LIGO II up to a distance of $\sim$100 kpc and with LIGO I to a distance of $\sim$5 kpc. If the core is nonrotating, its gravitational wave emission can be measured with LIGO II up to a distance of $\sim$15 kpc ($S/N \gtrsim 8$), while the signal from the Ledoux convection in the deleptonizing nascent neutron star can be detected up to a distance of $\sim$10 kpc ($S/N \gtrsim 8$). Both kinds of signals are generically produced by convection in any core-collapse supernova.

Subject headings: gravitational waves — hydrodynamics — relativity — supernovae: general

1. INTRODUCTION

For more than two decades astrophysicists have struggled to compute the gravitational wave signal produced by core-collapse supernovae (for a review, see, e.g., Müller 1997, p. 273). If the core collapse and/or the resulting supernova explosion involves time-dependent asphericities such that the third time derivative of the quadrupole moment of the mass-energy distribution is nonzero, part of the gravitational binding energy liberated in the event will be emitted in the form of gravitational waves. Such nonsphericities can be caused on large scales by the effects of rotation (Müller 1982; Finn & Evans 1990; Mönchmeyer et al. 1991; Yamada & Sato 1995; Zwerger & Müller 1997; Rampp, Müller, & Ruffert 1998; Dimmelmeier, Font, & Müller 2002; Fryer, Holz, & Hughes 2002; Fryer et al. 2003; Imamura, Pickett, & Durisen 2003; Ott et al. 2004; Shibata 2003) and low-mode convection (Herant 1995; Scheck et al. 2004), on small scales by flow fluctuations due to high-mode convection (Müller & Janka 1997; Fryer et al. 2003) and by anisotropic neutrino emission (Epstein 1978; Burrows & Hayes 1996; Müller & Janka 1997).

Theoretical predictions of the gravitational wave signal from core-collapse supernovae have been and still are hampered by the complex nature of the supernova explosion physics, which is not yet fully understood (Buras et al. 2003). Reliable simulations require realistic (rotating) precollapse stellar models, the incorporation of a realistic equation of state (EoS), a detailed modeling of weak interaction processes, Boltzmann neutrino transport, multidimensional hydrodynamics, and relativistic gravity. However, all past studies aimed at studying the gravitational wave signature of core-collapse supernovae have considered greatly simplified parameterized models involving one, several, or all of the following approximations: a polytropic equation of state, a simplified description of weak interactions and neutrino transport or none at all, parameterized precollapse stellar models, and Newtonian gravity (Müller 1982; Finn & Evans 1990; Mönchmeyer et al. 1991; Yamada & Sato 1995; Zwerger & Müller 1997; Rampp et al. 1998; Dimmelmeier et al. 2002; Fryer et al. 2002, 2003; Imamura et al. 2003; Kotake, Yamada, & Sato 2003; Ott et al. 2004; Shibata 2003). In addition, most of these simulations focused on the effects of rapid rotation and on the bounce signal covering the evolution up to only a few times 10 ms after core bounce.

From observations, as well as theoretical modeling, it is now commonly accepted that core-collapse supernovae do generically involve asphericities besides those expected in the case of a progenitor with a sufficiently rapidly rotating core (for a review, see, e.g., Müller 1998, p. 343). These asphericities are important or may be even essential for supernova dynamics (Herant et al. 1994; Burrows, Hayes, & Fryxell 1995; Janka & Müller 1996; Buras et al. 2003). Recent state-of-the-art axisymmetric two-dimensional simulations using a Boltzmann solver for the ν-transport (Rampp & Janka 2002; Buras et al. 2003) and simplified (as far as neutrino transport and neutrino-matter interactions are concerned) three-dimensional (Fryer & Warren 2002) simulations both confirm that convective overturn indeed occurs in the ν-heating region and is helpful for shock revival, thus making explosions possible even when spherically symmetric models fail (Janka & Müller

1996). However, despite strong convective action and a corresponding enhancement of the efficiency of neutrino energy transfer to the postshock matter, even the most realistic simulations of both nonrotating and rotating progenitor models up to now do not produce explosions (Buras et al. 2003). Multidimensional simulations further demonstrate that vigorous aspherical motion is unavoidable in the slowly deleptonizing and cooling proto–neutron star (Keil, Janka, & Müller 1996). Both the hot bubble convection (Müller & Janka 1997) and the convection in the proto–neutron star (see below), as well as the resulting anisotropic neutrino emission (Burrows & Hayes 1996; Müller & Janka 1997), give rise to an interestingly large gravitational wave signal.

Concerning consistent precollapse stellar models from evolutionary calculations of rotating stars, major progress has recently been achieved in the work of Heger, Langer, & Woosley (2000), who have performed what is up to now the most realistic evolutionary calculations for rotating massive stars to the onset of core collapse, including the effects of rotation, mixing, transport of angular momentum, and most recently, magnetic torques (Heger et al. 2004).[1] For the latter the central angular velocities become only on the order of 0.1 rad s^{-1}. Despite these fairly slow rotation rates the cores are still too fast to lead to typically expected neutron star natal spins, and angular momentum loss is considered a serious problem (Woosley & Heger 2004). The low iron core rotation rates, however, suggest that in spite of angular momentum conservation during core collapse, triaxial rotation-triggered instabilities need not be expected in the collapse simulations. For the time being, we therefore confine ourselves to axisymmetric models.

In the following we present the gravitational wave signatures of the currently most elaborate and detailed core-collapse supernova simulations. One of the models considered starts from an iron core with a rotation rate at the onset of collapse that is in the ballpark of predictions from the latest generation of stellar evolution models. The simulation also contains a state-of-the art description of neutrino-matter interactions and Boltzmann neutrino transport, a realistic equation of state, and two-dimensional axisymmetric hydrodynamics that takes into account general relativistic effects. We also present the gravitational wave signature of a state-of-the-art nonrotating supernova model. This model, which is based on another, less massive progenitor, serves to demonstrate that interesting gravitational wave signals can also be expected from nonrotating stars, which are strong enough to be detectable for supernovae that occur even at large distances in our Galaxy. Finally, we present the gravitational wave signal expected from the Ledoux convection in a proto–neutron star at times after the explosion has taken place ($\approx$1 s after core bounce).

The paper is organized as follows: In the next section we discuss the physics employed in our models and the numerical techniques used to perform the simulations. In § 3 we present the method used to extract the gravitational wave signature, and in § 4 we describe the results of our investigation. Finally, in § 5 we discuss the implications of our findings and give some conclusions.

2. INPUT PHYSICS AND NUMERICAL TECHNIQUES

For integrating the equations of hydrodynamics we employ the Newtonian finite-volume code PROMETHEUS (Fryxell, Müller, & Arnett 1989). This second-order, time-explicit Godunov code is a direct Eulerian implementation of the piecewise parabolic method (Colella & Woodward 1984) and is based on an exact Riemann solver.

We use spherical polar coordinates (r, θ, φ) and assume axial symmetry. However, motions in the φ-direction are allowed, and the azimuthal (rotational) velocity may be nonzero. In the rotating model the axis of rotation coincides with the axis of symmetry at $\theta = 0$. In this model we have also imposed equatorial symmetry. The two-dimensional computational grid consists of 400 logarithmically spaced zones in the radial direction and, if equatorial symmetry is assumed, of 64 equidistant angular zones covering an angular range $0 \leq \theta \leq \pi/2$. If equatorial symmetry is not assumed, the angular grid consists of 128 equidistant zones in the angular range $0 \leq \theta \leq \pi$.

The calculations are performed with the EoS of Lattimer & Swesty (1991) by using a value of the incompressibility of bulk nuclear matter of 180 MeV. This EoS is based on a compressible liquid drop model including nuclei, nucleons, electrons, positrons, and photons.

Neutrino transport is computed with the Boltzmann solver scheme described in detail in Rampp & Janka (2002) and Buras et al. (2003) for ν and $\bar{\nu}$ of all three flavors. For each angular bin of the numerical grid, the monochromatic moment equations for the radial transport of ν-number, energy, and momentum are solved. This set of equations is closed by a variable Eddington factor that is calculated from the solution of the Boltzmann equation on an angularly averaged stellar background. Beyond this "ray-by-ray" approach we also take into account the coupling of neighboring rays by lateral advection terms and ν-pressure gradients (Buras et al. 2003). For the transport an energy grid of 17 geometrically spaced bins is used with centers from 2 to 333 MeV.

The simulations were done with a Poisson solver that calculates the gravitational potential from the two-dimensional mass distribution. General relativistic effects are treated approximately by modifying the spherical part of the gravitational potential with correction terms due to the pressure and energy of the stellar medium and the neutrinos, which are deduced from a comparison of the Newtonian and relativistic equations of motion in spherical symmetry (Keil et al. 1996; Rampp & Janka 2002). The ν-transport contains gravitational redshift and time dilation but ignores the distinction between coordinate radius and proper radius. Comparison with fully relativistic, one-dimensional simulations showed that these approximations work well at least when the deviations of the metric coefficients from unity are moderate (M. Liebendörfer et al. 2004, in preparation).

We considered two (solar metallicity) progenitor models with main-sequence masses of 11.2 $M_\odot$ (Woosley, Heger, & Weaver 2002) and 15 $M_\odot$ (the stellar evolution model s15s7b2; S. E. Woosley 2003, private communication). The former progenitor was adopted as given by the stellar evolution calculation (model s11nr180), while angular momentum was added to the 15 $M_\odot$ progenitor (model s15r; see also Buras et al. 2003).

The angular frequency of the rotating model s15r (see Fig. 1) was assumed to be constant in the Fe and Si core and to decrease as $r^{-3/2}$ outside 1750 km (corresponding to a mass coordinate of 1.425 $M_\odot$, which is the inner edge of the O-rich silicon layer in the progenitor of model s15r). We have adopted a value of 0.5 s^{-1} for the central angular frequency. This ensures that the centrifugal force relative to the gravitational

[1] See also http://www.ucolick.org/~alex/stellarevolution.

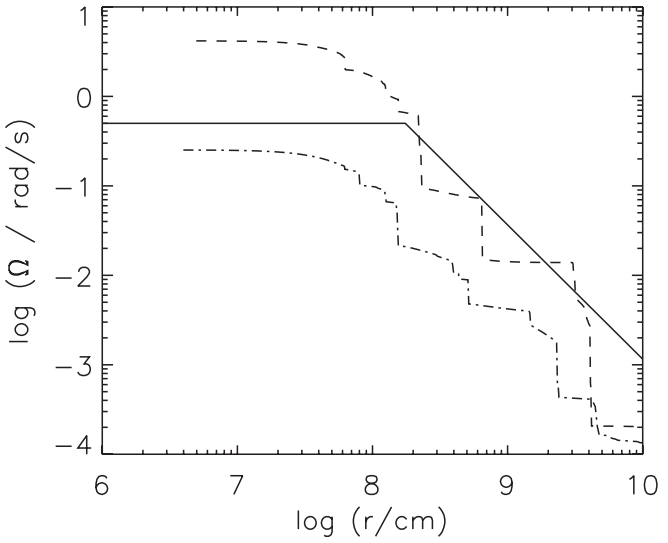

FIG. 1.—Angular velocity Ω as a function of radius r for the rotating 15 $M_\odot$ presupernova model (*dashed curve*) of Heger, Langer, & Woosley (2000), for the magnetic rotating 15 $M_\odot$ presupernova model (*dash-dotted curve*) of Heger et al. (2004), and for our rotating model s15r (*solid curve*).

force is below 0.7% everywhere in the inner part of the precollapse core and is roughly constant in the outer region of falling Ω. This smallness of the centrifugal force guarantees that the rotational deformation of the stellar core is initially negligibly small. As Figure 1 shows, inside the iron core ($r \lesssim 10^8$ cm) this rotation profile lies between the predictions from stellar evolution calculations of rotating (Heger et al. 2000) and magnetic rotating (Heger et al. 2004) presupernova models. Outside the iron core the rotation profile of our model s15r closely follows (on average) the profile of the rotating progenitor of Heger et al. (2000). Our choice of the angular velocity profile on the one hand maximizes rotational effects in view of the most recent evolution calculations for magnetized rotating massive stars. On the other hand, it avoids an extreme sub-millisecond period of the newly formed neutron star, as expected for even higher precollapse rotation rates. Even our rather modest initial core rotation leads to a neutron star spin period of only 1 ms in the most extreme case, that in which no angular momentum loss occurs and the neutron star contracts to a final radius of 10 km.

The initial value of the ratio of the rotational energy and the (absolute) gravitational binding energy is $\beta = 0.05\%$ in model s15r. This is a relatively small rotation rate compared with those typically assumed in parameter studies based on rotating polytropes (see, e.g., Zwerger & Müller 1997; Dimmelmeier et al. 2002; Ott et al. 2004). However, it is on the order of the largest rotation rates predicted by state-of-the-art evolutionary calculations of massive stars and even too fast with respect to observed rotation rates of young pulsars (Heger et al. 2004; see also § 5). Hence, as far as the state of rotation is concerned, our model is meant to represent not an extreme rare case but is in accord with the conditions in stellar iron cores expected from current models for the evolution of rotating massive stars. Because of the smallness of the assumed rotation rate we regarded it as unnecessary to relax the initial model into rotational equilibrium (the ratio between the centrifugal force and the gravitational force is below 1% in the progenitor model).

We have also analyzed a proto–neutron star model (pns180) that is the 180° analog of the model discussed in Keil et al. (1996), which covered an angular region of only 90°. Model pns180 provides complementary information about the gravitational wave signal expected from core-collapse supernovae, namely, the wave emission from the long-lasting (>1 s) nonradial motion driven by the deleptonization of the forming neutron star. The $\sim$1.1 $M_\odot$ convective core of the proto–neutron star of model pns180 was formed in the core collapse of a 15 $M_\odot$ star (Keil et al. 1996). Its evolution was followed by Keil (1997) for more than 1.2 s with a variant of the PROMETHEUS hydrodynamics code (see above), assuming axial symmetry and including a flux-limited (equilibrium) neutrino diffusion scheme, which was applied to each angular bin separately ("1.5D"). The computational grid consisted of 100 radial zones extending out to an initial radius of 58.8 km and 120 equidistant angular zones covering an angular range $0 \le \theta \le \pi$; i.e., no equatorial symmetry was assumed. During the simulated evolution the grid was contracted, and the neutron star shrank to a final radius of about 20 km (Keil et al. 1996).

3. CALCULATION OF THE GRAVITATIONAL WAVE SIGNATURE

The (quadrupole) gravitational wave amplitudes and energy spectra resulting from anisotropic mass motion are computed as described in Müller & Janka (1997, eqs. [10]–[12]) by using the Einstein quadrupole formula in the numerically convenient formulation derived by Blanchet, Damour, & Schäfer (1990) and by standard fast Fourier transform techniques. The wave amplitudes due to the anisotropic neutrino emission are obtained with the formalism given in Müller & Janka (1997, eqs. [28]–[31]), which is based on the work of Epstein (1978).

To find out whether the gravitational wave signals of our model stars (assumed to be located at some given distance) are detectable by terrestrial gravitational wave experiments, we have also computed the corresponding (optimal with respect to the relative orientation of source and detector) signal-to-noise (S/N) ratios obtained from matched filtering, which are determined by the relation

$$(\mathrm{S/N})^2 = 4 \int_0^\infty \frac{|\tilde{h}(\nu)|^2}{S_n(\nu)}\, d\nu, \tag{1}$$

where $\tilde{h}(\nu)$ is the Fourier transform of the gravitational wave amplitude $h(t)$ and $S_h(\nu)$, in Hz^{-1}, is the spectral density of the strain noise in the detector (Flanagan & Hughes 1998). Equation (1) can also be written as

$$(\mathrm{S/N})^2 = 4 \int_0^\infty \left[\frac{|\tilde{h}(\nu)|\nu^{1/2}}{h_{\mathrm{rms}}(\nu)}\right]^2 d\log\nu, \tag{2}$$

where $h_{\mathrm{rms}}(\nu)\ [\mathrm{Hz}^{-1/2}] \equiv [S_n(\nu)]^{1/2}$ is the spectral strain sensitivity (see, e.g., Fritschel 2002), which gives the rms noise level of the antenna at the frequency ν. The second expression for S/N (eq. [2]) is useful when discussing the spectra of the gravitational wave signals of our models (see § 4.2).

We point out here that matched filtering signal searches require a complete set of accurate theoretical wave templates. For core-collapse supernovae it is highly unlikely that one will ever possess such a precise prediction of the gravitational waveforms, as their details are influenced by the presence of stochastic processes (i.e., convective flows). In the absence of

templates one can rely instead on bandpass filtering or noise-monitoring, nonlinear filtering searches (Flanagan & Hughes 1998). While the gain in S/N obtainable from matched filtering compared with bandpass filtering is approximately the square root of the number of cycles in the wave signal, noise-monitoring, nonlinear filtering performs almost as well as matched filtering (Flanagan & Hughes 1998). Hence, the S/Ns computed according to equations (1)–(2) may be a bit too optimistic but should not be grossly overestimated.

In particular, we have determined the S/Ns of our models both for the Laser Interferometer Gravitational-Wave Observatory (LIGO) I and the tuned Advanced LIGO (LIGO II) interferometric gravitational wave detectors (Fritschel 2002). For LIGO I we used a fit to the strain sensitivity curve LIGO I SRD Goal available from the LIGO Web site.[2] In case of the tuned Advanced LIGO interferometer we have computed S/Ns for the three different strain sensitivity curves shown in Figure 2.

Concerning the sensitivity curves shown in this plot and some of our other figures, we point out that both the curves for LIGO II, as well as the curve for LIGO I, are for a *single* interferometer. In the case of LIGO I, there are two nominally identical 4 km instruments, plus a 2 km instrument at Hanford. This increases the net sensitivity by a factor $\sqrt{2}$ in the ideal case of statistical independence and Gaussian noise. For LIGO II, there are three interferometers (two at Hanford, one at Livingston). They could all be tuned the same way for a directed search or tuned differently. If all are tuned the same way, the net sensitivity is a factor $\sqrt{3}$ better at all frequencies than that of a single interferometer. The S/Ns given in this paper are for the complete detector, consisting of two interferometers (LIGO I) or three like-tuned interferometers (LIGO II).

Assuming axial symmetry and an observer located at an angle θ with respect to the symmetry axis of the source, the dimensionless gravitational wave amplitude $h(t)$ is related to the quadrupole wave amplitude A_{20}^{E2} (measured in centimeters), the lowest order nonvanishing term of a multipole expansion

[2] See http://www.ligo.caltech.edu/docs/G/G030014-00.

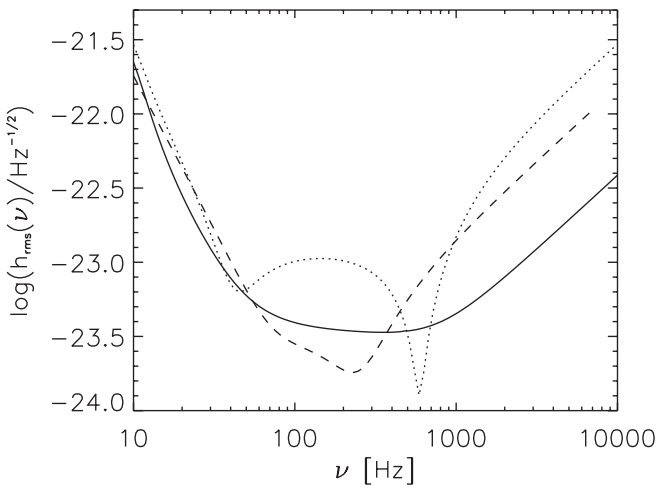

FIG. 2.—Strain sensitivity curves of the tuned Advanced LIGO interferometer (LIGO II) used in our analysis. The solid curve has an increased sensitivity at ∼1 kHz and a rather wide trough of nearly maximal sensitivity, while the dotted curve has a peak sensitivity of 1.2×10^{-24} at about 700 Hz and aligns with the peak in energy in some of our models (see § 4.2). The third sensitivity curve, the dashed curve, is tuned for sources that emit more at low frequencies (the so-called NS-NS–tuned instrument).

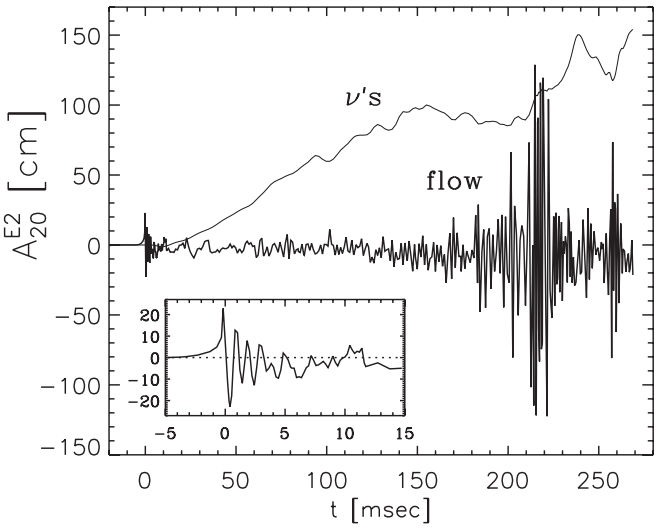

FIG. 3.—Gravitational wave quadrupole amplitude A_{20}^{E2} vs. time (post-bounce) due to convective mass flow and anisotropic neutrino emission (*thin line*) for the rotating delayed explosion model s15r of Buras et al. (2003). The inset shows an enlargement of the signal around the time of bounce.

of the radiation field into pure-spin tensor harmonics (see eq. [9] of Müller 1997, p. 273), according to

$$h = \frac{1}{8}\sqrt{\frac{15}{\pi}}\sin^2\theta\frac{A_{20}^{E2}}{R}, \tag{3}$$

where R is the distance to the source. In the following we always assume $\sin^2\theta = 1$.

4. RESULTS

4.1. *Wave Amplitudes*

The quadrupole wave amplitudes of models s15r, s11nr180, and pns180 are shown in Figures 3, 4, and 5, respectively. Besides the waveform resulting from the convective flow, each figure shows the signal due to the anisotropic neutrino emission. Insets further illustrate details of the wave signal for

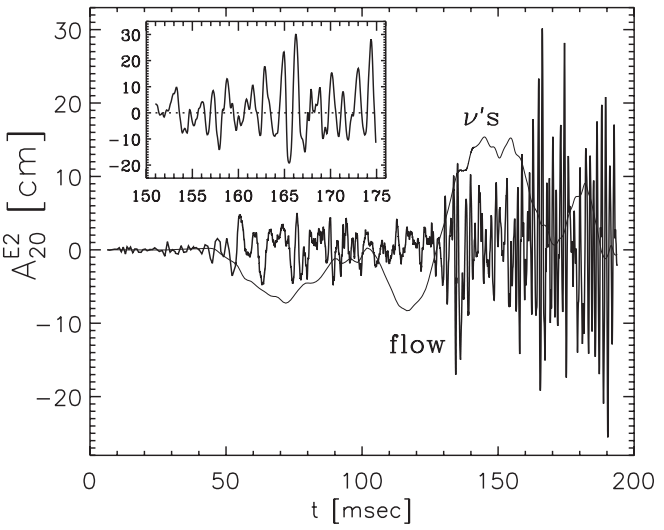

FIG. 4.—Same as Fig. 3 but for the delayed explosion model s11nr180 of Buras et al. (2003). The inset shows an enlargement of the signal between 150 and 175 ms after core bounce.

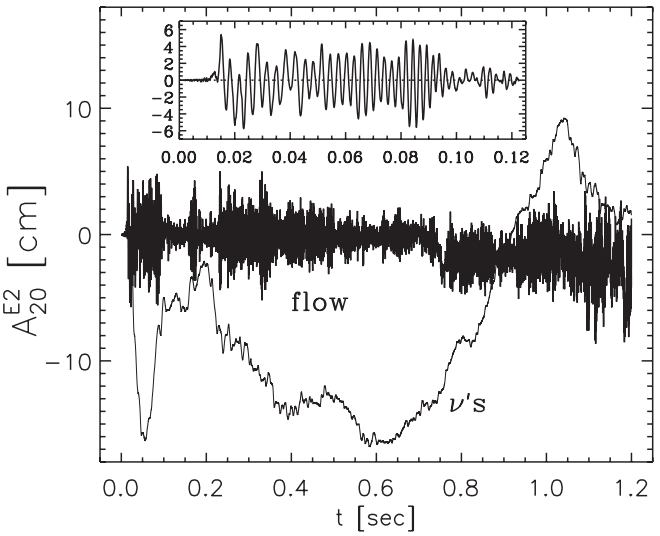

FIG. 5.—Same as Fig. 3 but for the proto–neutron star model pns180 of Keil (1997). Note that no bounce occurs in this model, which follows the neutrino cooling phase of the nascent neutron star. Time is measured from the start of the simulation at about 20 ms after stellar core collapse.

chosen periods of time and demonstrate that the wave signal consists of many quasi-periodic variations on timescales of a few milliseconds, which remain unresolved when the whole time evolution of the models is shown.

The quadrupole wave amplitude A_{20}^{E2} (eq. [2]) of model s15r at bounce is on the order of 20 cm showing (Fig. 3, *inset*) the typical prominent spike with the subsequent ring-down of a type I gravitational wave signal of a rotating core, which bounces because of the stiffening of the equation of state around nuclear matter density (Mönchmeyer et al. 1991). The postbounce wave amplitude stays below ~10 cm until about 150 ms, when convective mass motions driven by neutrino heating, in combination with the increasing rotation rate of the postshock region, amplify the wave signal. The growing rate of rotation of the postshock region is caused by the accretion of matter with higher angular momentum (as the initial rotation profile is constant to the edge of the Fe core) through the shock, and the specific angular momentum increases even beyond the edge of the iron core. The postshock region starts to exhibit large-scale nonradial pulsations (Fig. 6), which produce a long-term (~10–20 ms) variability on top of the rapidly varying (approximately millisecond) wave signal of up to 130 cm amplitude.

The nonrotating, hence initially spherically symmetric, model s11nr180 shows, as expected, no signal at bounce

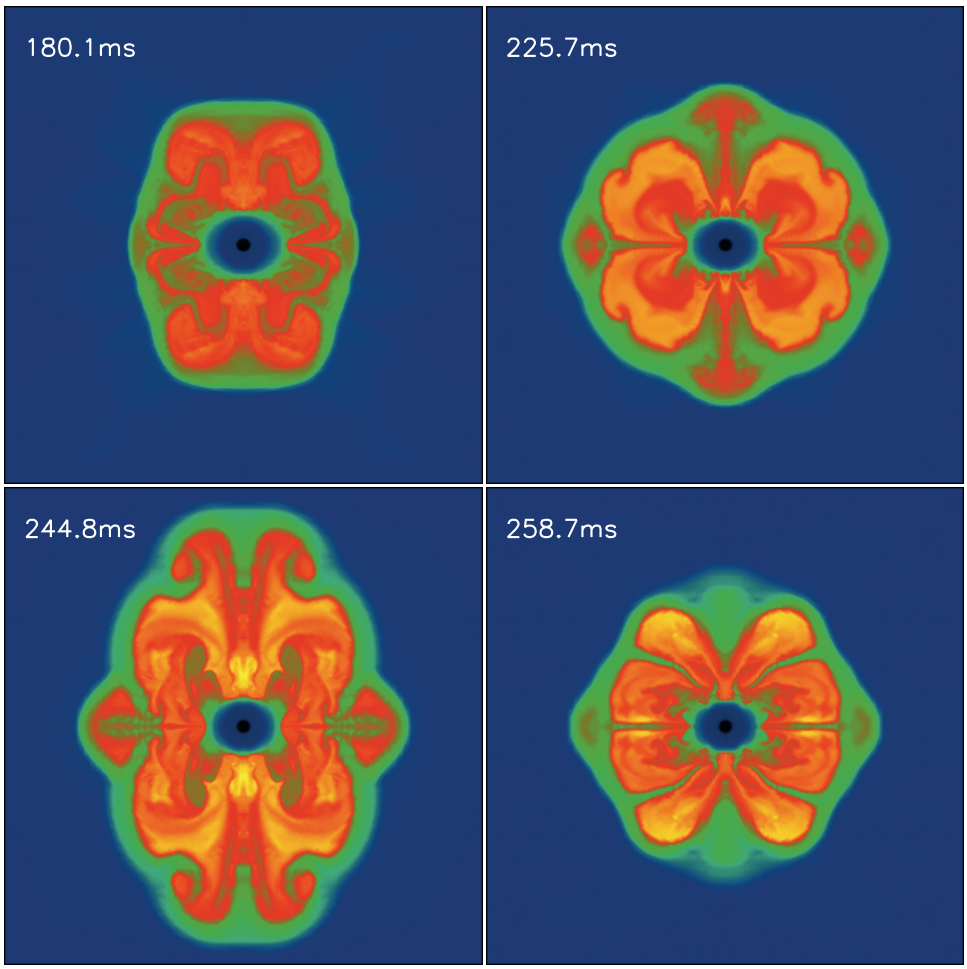

FIG. 6.—Four snapshots of the entropy distribution of the rotating delayed explosion model s15r of Buras et al. (2003). The side length of the plots is 600 km, and the numbers at top left in each panel give postbounce times. Bright regions are high-entropy bubbles. The shock is visible as the sharp deformed discontinuity, and the flattened proto–neutron star is the low-entropy oblate ellipse at the center.

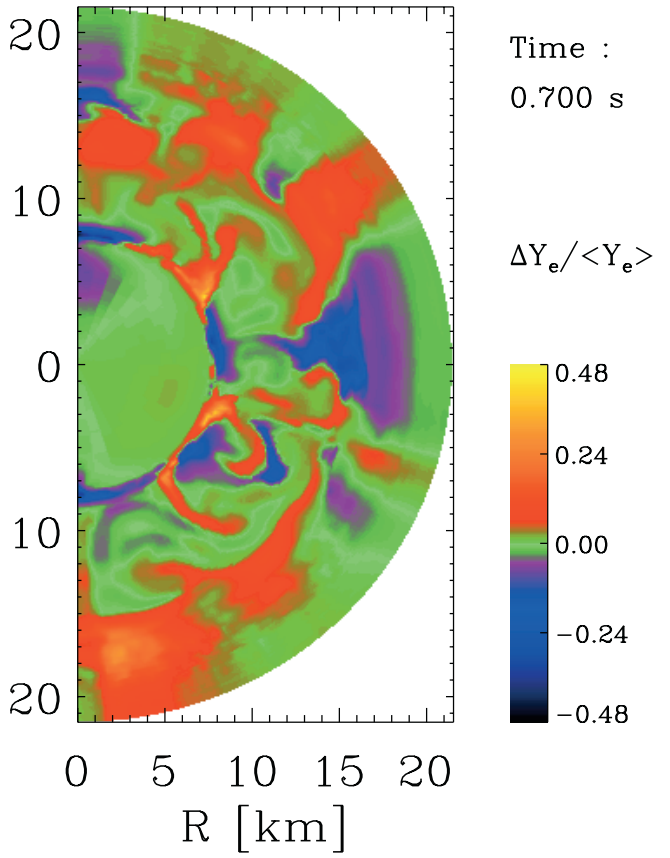

FIG. 7.—Relative variation of the proton-to-baryon ratio (electron number fraction) due to convective mass flow in the proto–neutron star model pns180 of Keil (1997) 0.7 s after core bounce. Proton-rich matter rises, while neutron-rich matter sinks inward.

(Fig. 4). Until 50 ms after bounce the wave amplitude of this model remains tiny (<1 cm). Only when the neutrino-driven convection sets in at around 40–50 ms does the wave amplitude grow to the size of a few centimeters. Eventually, as the convective activity becomes stronger, the maximum (absolute) amplitudes rise to values of several times 10 cm.

Neither model, the rotating (s15r) or the nonrotating one (s11nr180), explodes within the displayed time intervals. After an explosion has started, we expect a slow decay of the convective activity behind the expanding supernova shock, hence a declining gravitational wave amplitude from this region over a period of a few times 100 ms. The gravitational wave signal afterward will be dominated by the emission from convection *inside* the cooling nascent neutron star.

The proto–neutron star model exhibits a gravitational wave signal consisting of rapid (approximately millisecond) quasi-periodic temporal variations of roughly constant amplitude (on the order of centimeters) modulated on timescales of ∼100 ms (Fig. 5). While the former variations reflect mass motions and nonradial proto–neutron star oscillations occurring on the hydrodynamic (sound crossing) timescale, the long-term signal modulations are caused by the varying strength of the activity due to Ledoux convection in the proto–neutron star (Fig. 7).

The wave amplitude associated with anisotropic neutrino emission shows much less time structure and slower temporal variation than that produced by nonradial mass motion. It is characterized by an overall rise of the wave amplitude in the case of the rotating model s15r, a quasi-periodic oscillation with a timescale of ∼50 ms in the case of the nonrotating model s11nr180, and an even slower temporal variation (0.2–0.4 s) in the case of the proto–neutron star model pns180.

In the case of the rotating model (s15r) the temporal variation of the quadrupole wave amplitude of the neutrinos reflects the timescale of the large-scale, nonradial pulsations exhibited by the postshock region (∼10–20 ms; Fig. 6), while the short-term variations (approximately millisecond) of the wave amplitude of the mass flow are caused by the convective activity in the hot bubble region. The overall rise of the wave amplitude of the neutrinos is a consequence of the steadily increasing rotation rate (accretion of matter with higher angular momentum) and thus the growing rotational flattening of the nascent neutron star. In the nonrotating model (Fig. 4) and the proto–neutron star model (Fig. 5) the temporal variations of the wave amplitudes of the neutrinos are caused by large-scale localized neutrino-emitting downflows through the neutrino-heated bubble and by global changes in the location and shape of the convective emission regions, respectively.

4.2. *Wave Spectra and Signal-to-Noise Ratios*

In Figures 8–14 we show the (logarithm of the) quantity $|\tilde{h}(\nu)|\nu^{1/2}$ appearing in the numerator of equation (2). Each figure also gives $h_{\rm rms}(\nu)$, the rms noise level (see denominator of eq. [2]) of a LIGO I and a LIGO II single interferometer (see § 3) as a function of the frequency ν, the LIGO II curve being the solid curve of Figure 2. Both quantities determine the S/N, which is given for all models and both antennas in Table 1, using again the sensitivity curve (*solid curve*) of Figure 2. We remind the reader that the S/N values are computed for the complete LIGO I and LIGO II detectors as explained in § 3.

The spectrum of the complete wave train of model s15r caused by both anisotropic mass flow and neutrino emission is displayed in Figure 8 for a supernova at a distance of 10 kpc. It rises to a broad peak between ∼600 and ∼700 Hz and then declines rapidly at higher frequencies. The figure indicates that while the S/N is probably too small for this event to be detectable by LIGO I, it could be very well detected by LIGO II. This is confirmed by the S/Ns computed from equation (2) (using the sensitivity curve of Fig. 2, *solid curve*), which are 3.7 and 67 for the LIGO I and LIGO II detectors, respectively (Table 1). Even at a distance of 100 kpc the S/N is still ≈7 for LIGO II; i.e., it is probably sufficiently large for a detection of the event (Flanagan & Hughes 1998). Comparing Figure 8 with Figure 9, which shows the spectrum resulting from anisotropic neutrino emission alone, one recognizes that the low-frequency part of the spectrum (below ∼100 Hz) is dominated by the contribution of the neutrinos, because their

TABLE 1
SIGNAL-TO-NOISE RATIOS FOR LIGO I AND II

Model	D[a] (kpc)	S/N I	S/N II	$E_{\rm GW}$[b] ($M_\odot c^2$)
s15r.....	10	3.7	67	3.0×10^{-09}
s15r bnc[c]	3	0.7	14	3.6×10^{-11}
s11nr180.....	10	0.6	13	1.9×10^{-10}
pns180.....	10	0.4	8	1.6×10^{-10}

NOTE.—For complete instruments with multiple antennas.
[a] Source distance.
[b] Radiated gravitational wave energy.
[c] Only bounce signal of model s15r.

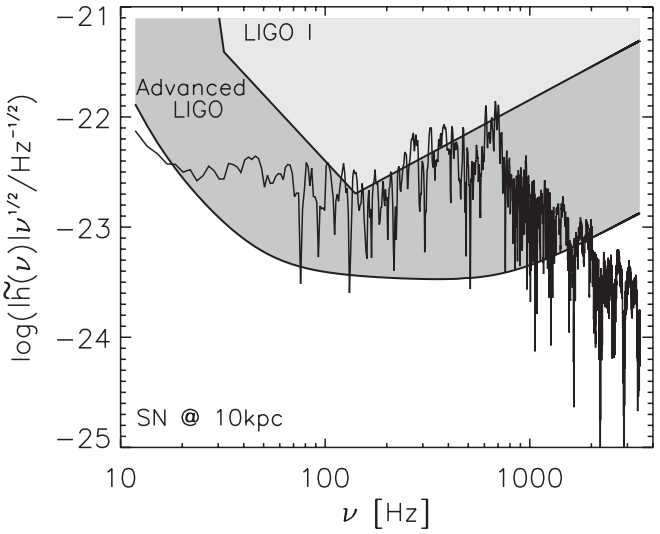

FIG. 8.—Spectral energy distribution of the quadrupole radiation due to convective mass flow and anisotropic neutrino emission for the rotating delayed explosion model s15r of Buras et al. (2003) as a function of frequency of the emitted gravitational radiation for a supernova at a distance of 10 kpc.

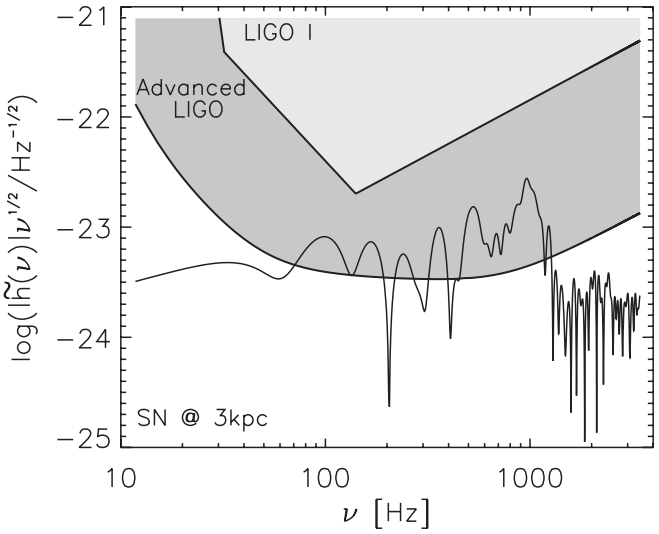

FIG. 10.—Same as Fig. 8 but only for the bounce signal, and a supernova at a distance of 3 kpc.

quadrupole wave amplitude varies on much longer timescales than that of the mass flow (Fig. 3).

When we Fourier-transform just the bounce signal (Fig. 3, *inset*), i.e., the wave signal up to 15 ms past core bounce, we find that its spectrum peaks at a somewhat higher frequency of $\sim$900 Hz (Fig. 10) than that of the complete signal. The S/Ns drop to 0.7 (LIGO I) and 14 (LIGO II) even when the source is located at the smaller distance of 3 kpc (Table 1).

The spectrum of the nonrotating model s11nr180 (Fig. 11) is qualitatively quite similar to that of the rotating model s15r (Fig. 8), but the corresponding S/Ns are much smaller for a source located at the same distance (10 kpc): $S/N = 0.6$ (LIGO I) and $S/N = 13$ (LIGO II), respectively (Table 1). Thus, while a nonrotating supernova (model s11nr180) is detectable with LIGO II up to a distance of $\sim$15 kpc, a massive star rotating at a rate in the ballpark predicted by state-of-the-artstellar evolution models produces a gravitational wave supernova signal that can clearly be seen by LIGO II throughout the Galaxy and in the Magellanic Clouds and by LIGO I if the supernova occurs less than $\sim$5 kpc away from Earth, a distance limit that encompasses all historical Galactic supernovae. As in the case of the rotating model, the low-frequency part of the spectrum of model s11nr180 is dominated by the contribution from anisotropic neutrino emission (Fig. 12) because of the slower temporal variation of the corresponding quadrupole wave amplitude (Fig. 4).

According to our results the "long term" ($\gtrsim$1 s) gravitational wave signal produced by all core-collapse supernova events due to convective activity inside the proto–neutron star is detectable with LIGO II ($S/N = 8$) up to a distance of 10 kpc (Fig. 13; Table 1). The spectrum displays a narrow dominant peak at $\sim$1.3 kHz and two additional, weaker broad maxima centered at 1 kHz and $\sim$350 Hz. Anisotropic neutrino emission again dominates the spectrum at frequencies below $\sim$100 Hz (Fig. 14). We point out here that the convective

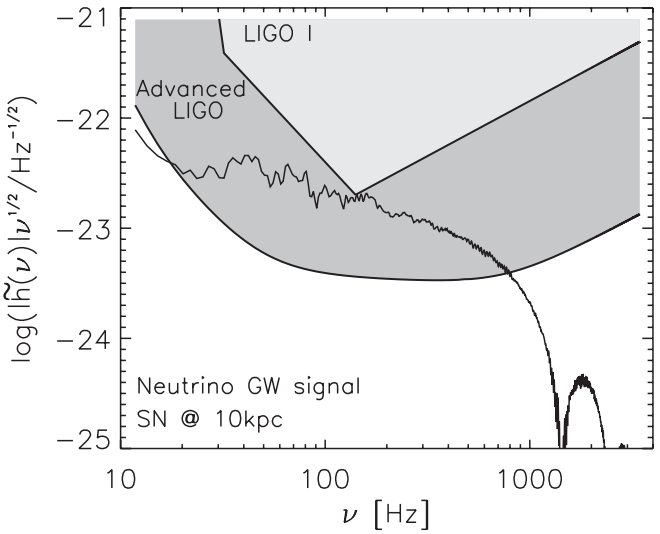

FIG. 9.—Same as Fig. 8 but showing only the contribution due to anisotropic neutrino emission.

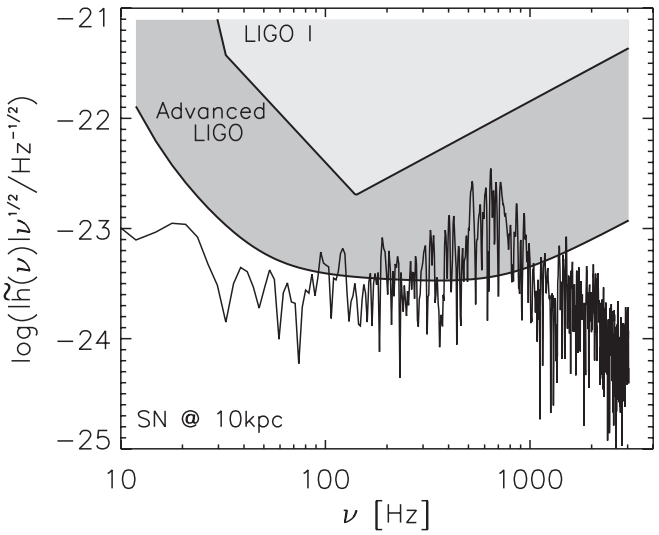

FIG. 11.—Same as Fig. 8 but for the delayed explosion model s11nr180 of Buras et al. (2003).

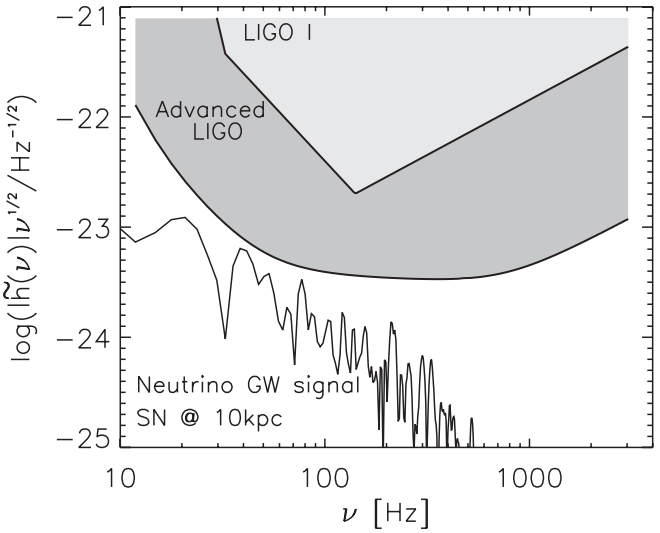

FIG. 12.—Same as Fig. 9 but for the delayed explosion model s11nr180 of Buras et al. (2003).

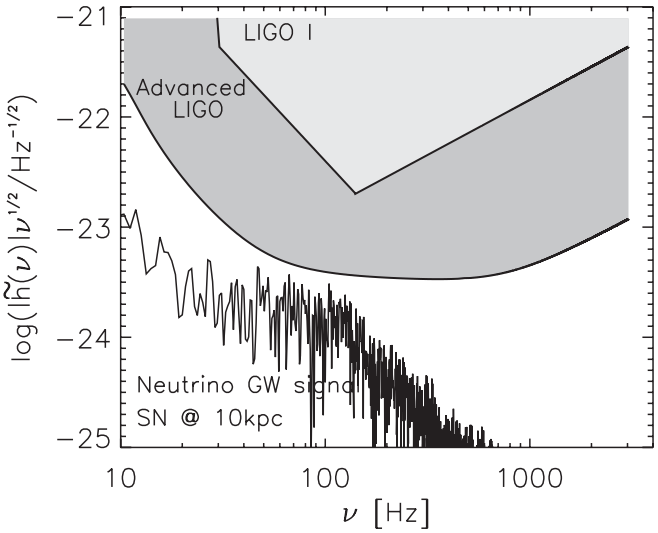

FIG. 14.—Same as Fig. 9 but for the proto–neutron star model pns180 of Keil (1997).

activity in the proto–neutron star may continue beyond the time period covered by our simulation, perhaps lasting more than 10 s, until the deleptonization is complete and the convective motion is damped by viscous effects. Assuming that the amplitude and the spectrum of the gravitational wave emission do not change considerably during this time, the S/Ns quoted for this model in Table 1 may increase by a factor of $\gtrsim$10, as they depend linearly on the size of the Fourier amplitude, which grows proportionally with the length of the signal.

The S/Ns given in Table 1 for the complete tuned Advanced LIGO depend somewhat, but not excessively, on the choice of the sensitivity curve. In the case of model s15r the S/N increases only slightly from 67 to 71 and 70 when using the dotted and dashed curves of Figure 2, respectively. The corresponding S/Ns for model s11nr180 are 13, 17, and 10, respectively, and those for model pns180 are 8, 5, and 8, respectively. Hence, for the latter two models, tuning the sensitivity curve for source optimization can increase the S/N values by up to 70%.

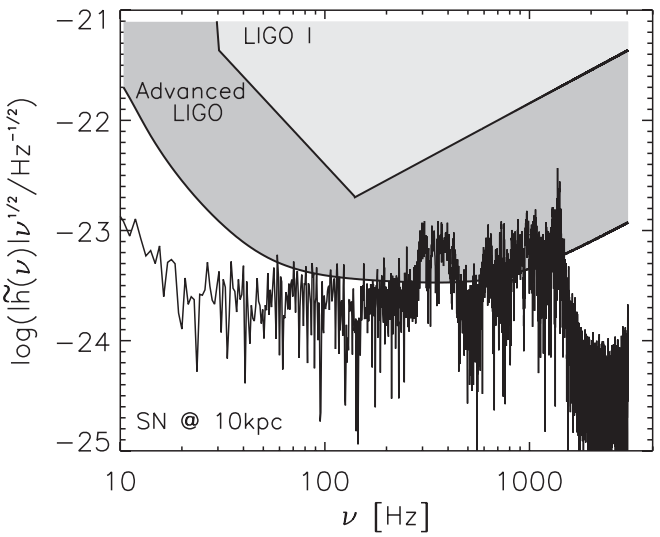

FIG. 13.—Same as Fig. 8 but for the proto–neutron star model pns180 of Keil (1997).

4.3. *Amount of Radiated Energy*

The energy radiated in the form of gravitational waves is given by

$$E_{\mathrm{GW}} = \frac{c^3}{G}\frac{1}{32\pi}\int_{-\infty}^{\infty}\left[\frac{dA_{20}^{E2}(t)}{dt}\right]^2 dt \tag{4}$$

$$= \frac{c^3}{G}\frac{1}{16\pi}\int_{0}^{\infty}|\tilde{A}_{20}^{E2}(\nu)|^2\nu^2 d\nu, \tag{5}$$

where $\tilde{A}_{20}^{E2}$ is the Fourier transform of A_{20}^{E2} and c and G are the speed of light in vacuum and Newton's gravitational constant, respectively (see e.g., eqs. [22], [26], and [28] in Zwerger & Müller 1997). We used both expressions above to compute the radiated energy and found for all three models very good agreement, with numerical differences only in the few percent range.

Our analysis implies that nonspherical core-collapse supernovae rotating with rates in the ballpark predicted by state-of-the-art evolutionary calculations of massive stars emit an energy of a few times $10^{-9}\ M_\odot\ c^2$ (where $M_\odot$ is the solar mass) in the form of gravitational radiation (Table 1). This number might increase for stars more massive than the 15 $M_\odot$ progenitor we have considered and is reduced by roughly 1 order of magnitude when nonrotating cores or the emission of convective proto–neutron stars are considered. Anisotropic neutrino emission does not contribute much to the amount of radiated energy, as the corresponding quadrupole wave amplitudes show a slower and smaller temporal variation than those due to the nonspherical mass flow.

5. DISCUSSION AND CONCLUSIONS

We have presented the gravitational wave signature of core-collapse supernovae by using the most realistic input physics available at present. Our analysis is based on state-of-the-art progenitor models of rotating and nonrotating massive stars, whose axisymmetric core collapse is simulated by integrating the hydrodynamic equations, together with the Boltzmann

equation for the neutrino transport, including an elaborate description of neutrino interactions, and a realistic equation of state. We have computed the quadrupole wave amplitudes, the Fourier wave spectra, the amount of energy radiated in the form of gravitational waves, and the S/Ns for the LIGO I and LIGO II detectors resulting from both nonradial mass motion and anisotropic neutrino emission.

The results show that the dominant contribution to the gravitational wave signal is not produced by the core bounce itself but instead by the neutrino-driven convection in the postshock region, which lasts up to several hundred ms postbounce. This finding is qualitatively different from that of previous core-collapse simulations that have been performed with greatly simplified parameterized models involving (1) a polytropic equation of state, and/or (2) a simplified description of weak interactions and neutrino transport or none at all, and/or (3) parameterized precollapse stellar models with sometimes extreme rotation rates, and/or (4) Newtonian gravity.

There are basically two reasons for our result. On the one hand, the most recent evolution calculations of magnetized rotating massive stars predict relatively low rotation rates for precollapse stellar cores. This rather slow rotation, in combination with the realistic equation of state, reduces the importance of the gravitational wave signal from the core bounce. On the other hand, the explosion of massive stars should start with some time delay (a tenth or a few tenths of a second) after core bounce, possibly driven by the neutrino-heating mechanism, which is supported by very strong postshock convection. Such a longer time delay seems to be favored by observed neutron star masses (which are not compatible with rapid explosions), by nucleosynthesis constraints, and, last but not least, by the fact that vigorous convection can develop only on longer timescales ($\gtrsim$0.1 s) and should reach its maximum strength around the time when the explosion is launched and gains momentum. The latter fact increases the importance of the associated gravitational wave emission.

We further find that the contribution to the signal from anisotropic neutrino emission is dominant at frequencies below $\sim$100 Hz, while nonspherical mass flow is the dominant contribution in the range between $\sim$300 and $\sim$1200 Hz. Besides the neutrino-driven convection in the postshock region, the Ledoux convection inside the deleptonizing proto–neutron star also gives rise to an important gravitational wave signal from core-collapse supernovae.

For a stellar iron core rotating with a central angular frequency of 0.5 s^{-1}, which is relatively small compared with the rotation rates typically assumed in parameter studies based on rotating polytropes (see, e.g., Zwerger & Müller 1997; Dimmelmeier et al. 2002; Ott et al. 2004) but which is on the order of the largest rotation rates predicted by state-of-the-art evolutionary calculations of massive stars (Heger et al. 2004), the core bounce signal would be detectable (S/N $\gtrsim$ 7) with LIGO II for a supernova up to a distance of $\sim$5 kpc. However, the signal caused by neutrino-driven convection is observable with LIGO II up to a distance of $\sim$100 kpc, and even with LIGO I to a distance of $\sim$5 kpc.

Because of the smallness of the assumed initial rotation rate, we do not expect any significant growth of nonaxisymmetric instabilities (e.g., bar modes) even after core collapse when angular momentum conservation leads to a spin-up of the core. For the same reason also no centrifugal hang-up but a regular bounce occurs at about nuclear matter density. Consequently, the gravitational wave (bounce) signal is not of type II, consisting of several distinct spikes, but of type I, having one prominent spike at bounce followed by a ring-down (Mönchmeyer et al. 1991).

As far as the initial state of rotation is concerned, our model does not represent an extreme, rare case but is in accord with more typical iron core conditions, as expected from the evolution of rotating massive stars. We point out here that most models used in previous investigations have rotational rates that are too large in comparison with those observed for newborn pulsars (see, e.g., Kotake et al. 2003). Even our initially quite slowly rotating model produces a pulsar spinning with period $P_{\rm rot}$ between 1 and 2 ms (depending on its final radius of 10–15 km and assuming angular momentum conservation in the neutron star after the end of our simulations), which is not far from the breakup limit. Millisecond pulsars have rotational energies $\sim 5 \times 10^{52}$ ergs $(P_{\rm rot}/1\ {\rm ms})^{-2}$ $(R/10\ {\rm km})^2 M/(1.5\ M_\odot)$. If such rapid rotators have to be slowed down to match the rotation rates of observed young pulsars, which is difficult to achieve on short timescales (Woosley & Heger 2004), the question arises, Where has all this rotational energy gone, if it is not observable in kinetic energy or electromagnetic radiation from the supernova or pulsar? Neither do R-modes appear now as a likely energy drain (Arras et al. 2003).

If the core is nonrotating (model s11nr180), its gravitational wave signal due to aspherical motion in the neutrino-heated bubble and due to anisotropic neutrino emission is detectable (S/N $\gtrsim$ 8) with LIGO II up to a distance of $\sim$15 kpc, while the signal from the Ledoux convection (model pns180) in the deleptonizing proto–neutron star can be measured at least to a distance of $\sim$10 kpc. Both kinds of signals are generically produced in any core-collapse supernova.

As our models are axisymmetric, the results may change when three-dimensional effects associated with the convection inside the proto–neutron star and in the hot bubble region are included. Both phenomena are genuinely three-dimensional. In this respect the simulations of Fryer & Warren (2002) and their analysis of the gravitational wave emission (Fryer et al. 2003) may provide an answer to this uncertainty in our results. These authors find that the size and dynamics of the convective structures are similar to those in axisymmetric simulations.

Finally, we want to mention another mechanism that causes a gravitational wave signal in core-collapse explosions. Recent simulations by Scheck et al. (2004) indicate that the proto–neutron star is accelerated during the explosion at a rate up to $\sim$3000 km s^{-2}, resulting in large kick velocities in some models. The acceleration can be caused either by asymmetric accretion onto the proto–neutron star or by the pull of the gravitational potential of matter distributed asymmetrically in the surrounding hot bubble region. Because of the erratic behavior of the accretion downflows, the acceleration can temporarily change sign, leading to an additional oscillatory component superposed on or preceding the steady acceleration component.

An order-of-magnitude estimate of the resulting scale of the gravitational wave signal can be obtained by approximating the proto–neutron star by a point mass M (initially at rest), which, e.g., moves in the positive z-direction starting at $z = 0$. If the point mass experiences a constant acceleration b for a time t, its displacement is given by $z(t) = (b/2)t^2$. The only nonvanishing (Cartesian) component of the time-dependent quadrupole moment (measured with respect to the origin of the coordinate system) of such a moving point mass is $Q_{zz} = \frac{2}{3} M z^2(t) = \frac{1}{6} M b^2 t^4$. The lowest (quadrupole) order

contribution to the gravitational wave luminosity $L \equiv dE_{\rm GW}/dt$ of such a moving point mass is due to the temporal variation of its quadrupole moment (Thorne 1980) and is given by $L_{\rm kick} = [G/(5c^5)]\langle (d^3Q_{zz}/dt^3)^2\rangle = [16G/(5c^5)]M^2b^4t^2$, which can be written as

$$L_{\rm kick} = 2.0 \times 10^{-19}\left(\frac{M}{1\ M_\odot}\right)^2 b_2^4 t^2 \frac{M_\odot\ c^2}{1\ \rm s}, \qquad (6)$$

where b_2 is the acceleration in units of 10^2 km s^{-2} and t the time of acceleration measured in seconds. If the motion of the point mass (initially at rest at $z = 0$) is caused by a periodic acceleration of amplitude A and timescale τ, i.e., $d^2z(t)/dt^2 = A\cos(2\pi t/\tau)$, the resulting gravitational wave luminosity is given by $L_{\rm osc} = (2G/9\pi^2c^5)M^2A^4\tau^2$ or by

$$L_{\rm osc} = 1.4 \times 10^{-19}\left(\frac{M}{1\ M_\odot}\right)^2 A_3^4 \tau_{-1}^2 \frac{M_\odot\ c^2}{1\ \rm s}, \qquad (7)$$

where A_3 is the acceleration in units of 10^3 km s^{-2} and τ_{-1} is the oscillation timescale, measured in units of 10^{-1} s. From their simulations Scheck et al. (2004) infer $b_2 \lesssim 5$, $t \approx 1$, $A_3 \lesssim 3$, and $\tau_{-1} \approx 1$ for the proto–neutron star of mass $M \sim 1\ M_\odot$. Hence, the gravitational wave signal from the acceleration giving rise to the kick of the proto–neutron star is quite small ($L_{\rm kick} \lesssim 10^{-16}$, in $M_\odot\ c^2$ s^{-1}), and the signal from the oscillatory motion of the proto–neutron star is even smaller ($L_{\rm osc} \lesssim 10^{-17}$, in $M_\odot\ c^2$ s^{-1}). The former signal is expected to have a typical frequency of approximately 1 Hz, and the latter one should be dominant at about 10–20 Hz.

Both signals are very small compared with the signal caused by the bounce of a rotating core, because the accelerations encountered during core bounce are much larger. The accelerations, which cause the varying quadrupolar deformation of the rotating core, are on the order of 10^6 km s^{-2}; i.e., they are roughly a factor of 10^3 larger than those producing the kick or the oscillatory motion of the proto–neutron star. These accelerations act for only $\sim$10 ms (the damping timescale of the postbounce ringing; see, e.g., Fig. 3, *inset*), which is a factor of $\sim$100 ($\sim$10) shorter than t (τ_{-1}), and involve a mass of only $\sim$0.1 $M_\odot$, which is a factor $\sim$10 smaller than M. Nevertheless, as L scales bi-quadratically with the acceleration and only quadratically with the mass and timescale (see eqs. [6] and [7]), the gravitational wave luminosity of rotational core bounce exceeds that of the proto–neutron star (kick and oscillatory) motion by a factor $\sim 10^6$–10^8.

The authors would like to thank W. Keil for computing the proto–neutron star model used in our analysis. Support by the Sonderforschungsbereich 375 on astroparticle physics and the Sonderforschungsbereich/Transregio 7 on gravitational wave astronomy of the Deutsche Forschungsgemeinschaft is acknowledged. One of the authors (D. H. S.) was supported by National Science Foundation grant PHY 01-07417. The simulations were performed at the Rechenzentrum Garching of the Max-Planck-Society.

REFERENCES

Arras, P., Flanagan, E. E., Morsink, S. M., Schenk, A. K., Teukolsky, S. A., & Wasserman, I. 2003, ApJ, 591, 1129
Blanchet, L., Damour, T., & Schäfer, G. 1990, MNRAS, 242, 289
Buras, R., Rampp, M., Janka, H.-T., & Kifonidis, K. 2003, Phys. Rev. Lett., 90, 241101
Burrows, A., & Hayes, J. 1996, Phys. Rev. Lett., 76, 352
Burrows, A., Hayes, J., & Fryxell, B. A. 1995, ApJ, 450, 830
Colella, P., & Woodward, P. R. 1984, J. Comput. Phys., 54, 174
Dimmelmeier, H., Font, J. A., & Müller, E. 2002, A&A, 393, 523
Epstein, R. 1978, ApJ, 223, 1037
Finn, L. S., & Evans, C. R. 1990, ApJ, 351, 588
Flanagan, E. E., & Hughes, S. A. 1998, Phys. Rev. D, 57, 4535
Fritschel, P. 2002, Proc. SPIE, 4856, 282
Fryer, C. L., & Warren, M. S. 2002, ApJ, 574, L65
Fryer, C. L., Holz, D. E., & Hughes, S. A. 2002, ApJ, 565, 430
Fryer, C. L., Holz, D. E., Hughes, S. A., & Warren, M. S. 2003, preprint (astro-ph/0211609)
Fryxell, B. A., Müller, E., & Arnett, W. D. 1989, preprint (MPA-449)
Heger, A., Langer, N., & Woosley, S. E. 2000, ApJ, 528, 368
Heger, A., Woosley, S. E., Langer, N., & Spruit, H. 2004, in IAU Symp. 215, Stellar Rotation, ed. A. Maeder & P. Eenens (San Francisco: ASP), in press (astro-ph/0301374)
Herant, M. 1995, Phys. Rep., 256, 117
Herant, M., Benz, W., Hix, W. R., Fryer, C. L., & Colgate, S. A. 1994, ApJ, 435, 339
Imamaura, J. N., Pickett, B. K., & Durisen, R. H. 2003, ApJ, 587, 341
Janka, H.-Th., & Müller, E. 1996, A&A, 306, 167
Keil, W. 1997, Ph.D. thesis, Technical Univ. Munich
Keil, W., Janka, H.-Th., & Müller, E. 1996, ApJ, 473, L111
Kotake, K., Yamada, S., & Sato, K. 2003, Phys. Rev. D, 68, 044023
Lattimer, J. M., & Swesty, F. D. 1991, Nucl. Phys. A, 535, 331
Mönchmeyer, R., Schäfer, G., Müller, E., & Kates, R. 1991, A&A, 246, 417
Müller, E. 1982, A&A, 114, 53
———. 1997, in Relativistic Gravitation and Gravitational Radiation, ed. J.-A. Marck & J.-P. Lasota (Cambridge: Cambridge Univ. Press), 273
———. 1998, in Computational Methods for Astrophysical Fluid Flow, ed. O. Steiner & A. Gautschy (Berlin: Springer), 343
Müller, E., & Janka, H.-Th. 1997, A&A, 317, 140
Ott, C. D., Burrows, A., Livne, E., & Walder, R. 2004, ApJ, 602, 834
Rampp, M., & Janka, H.-Th. 2002, A&A, 396, 361
Rampp, M., Müller, E., & Ruffert, M. 1998, A&A, 332, 969
Scheck, L., Plewa, T., Janka, H.-T., Kifonidis, K., & Müller, E. 2004, Phys. Rev. Lett., 92, 011103
Shibata, M. 2003, Phys. Rev. D, 67, 024033
Thorne, K. S. 1980, Rev. Mod. Phys., 52, 285
Woosley, S. E., & Heger, A. 2004, in IAU Symp. 215, Stellar Rotation, ed. A. Maeder & P. Eenens (San Francisco: ASP), in press (astro-ph/0301373)
Woosley, S. E., Heger, A., & Weaver, T. A. 2002, Rev. Mod. Phys., 74, 1015
Yamada, S., & Sato, K. 1995, ApJ, 450, 245
Zwerger, T., & Müller, E. 1997, A&A, 320, 209